NUMERICAL AND EXPERIMENTAL STUDY OF A FLAT PLATE SOLAR COLLECTOR WITH TRANSPARENT INSULATION AND OVERHEATING PROTECTION SYSTEM

Hamdi Kessentini, Roser Capdevila, Jesus Castro and Assensi Oliva

Centre Tecnològic de Transferència de Calor (CTTC)
Universitat Politècnica de Catalunya (UPC)
ETSEIAT, C. Colom 11, 08222 Terrassa (Barcelona), Spain
Fax: +34 93 739 89 20 e-mail: cttc@cttc.upc.edu

1. Introduction

Flat plate solar collectors (FPSC) are generally designed for applications with typical working temperatures between 40 and 60°C which is mainly the case of domestic hot water systems. Beyond this, a large industrial application potential exists for solar heat at medium temperature level (80-160°C). In fact, about 50% of the industrial heat demand is within this temperature range. Solar cooling and air conditioning systems also need heat at medium temperature levels. Solar drying of wood, crops, fruits, sterilizing, washing, cleaning, etc., distillation and desalination are other application potentials for medium temperature heat (Schweiger 1997).

The standard solar collectors able to produce heat at required temperatures above 80°C with reasonable efficiency (e.g. Evacuated tubes, Compound Parabolic Collectors (CPC), Parabolic Trough Collectors (PTC)) are too expensive to compete with conventional energy sources.

Reduction of the heat losses from the absorber to ambient is a major concern for FPSC. Selective coatings techniques were developed to reduce thermal radiation heat transfer from the absorber while preserving high absorptance. In the last two decades, prototypes of flat plate collectors with transparent insulation material (TIM) were developed and tested (Platzer 1992a, Schweiger 1997). The test results were encouraging as a low cost alternative was obtained and a performance comparable to that of evacuated tubes collectors was ensured (Rommel and Wagner, 1992, Goetzberger and Rommel, 1987).

This type of FPSC with TIM can be fabricated by the same way as the conventional FPSC but by inserting a transparent insulation material (TIM) glued under the glass cover. By this way, both natural convection and radiation heat losses from the top of the collector are significantly reduced. Consequently, a FPSC equipped with HTIM has lower coefficient of heat losses and thus can give higher performance than a simple FPSC.

FPSC with TIM can reach very high temperatures especially in periods of little or no hot water consumption or in case of the pump failure. Under these conditions, they may reach stagnation temperatures exceeding 290°C. Under the aforementioned stagnation conditions, the solar collector can not deliver the absorbed solar radiation to the transfer fluid which leads to increasing its temperature above a desired maximum level. This high temperature can damage the collector components and especially the TIM and even cause the degradation or boiling of the circulating fluid.

TIM generally made from plastics (Kaushika 2003) cannot withstand this high stagnation temperatures and melt when reaching temperature above 140°C, depending on the TIM. That is why, this type of solar collectors must be equipped with an overheating protection system whose function is to prevent the TIM from reaching high temperatures. This is one of the main technical challenges of this work.

In this paper a FPSC with TIM and an overheating protection system is investigated numerically and experimentally. The studied collector has been manufactured using a process similar to that of the conventional FPSC but by inserting a honeycomb TIM glued under the glass cover. The designed overheating protection system consists of a ventilation channel inserted between the absorber and the back insulation and has a thermally actuated door which opens when it reaches a specific temperature and remains closed otherwise. This system is designed to protect the collector when reaching stagnation conditions while preserving good performances during normal operations.

The developed numerical model within this work uses a multi-layer approach permitting to solve the different phenomenologies taking place in each element of the collector. The resolution of the TIM, which represents the most complicated component of the collector, is carried out by means of a high level model allowing to simulate the TIM behavior by means of resolution of the Radiative Transfer Equation in three dimensional coordinate system.

2. Technical description of the designed solar collector

2.1. Design of the prototype solar collector

The constructed solar collector has a total aperture area A=2.24 m^2 and a thickness of 157 mm. A cross section of the solar collector is shown in figure 1. It consists of a glass cover, TIM, air gap under the TIM, absorber, air channel located under the absorber, back and edge insulation and casing.

The absorber plate is composed of 8 copper fins welded directly to riser copper tubes. The absorber coating is selective (α=0.95, ε=0.5) and black chrome. The used glass is low iron of thickness 4 mm. The used TIM is slat structure with 4mm as thickness and maximum temperature resistance 140°C ± 10%. The gluing of the TIM to the glass cover is carried out by means of a high temperature resistant transparent adhesive. The back and lateral insulation used for the solar collector is rigid panel rock wool.

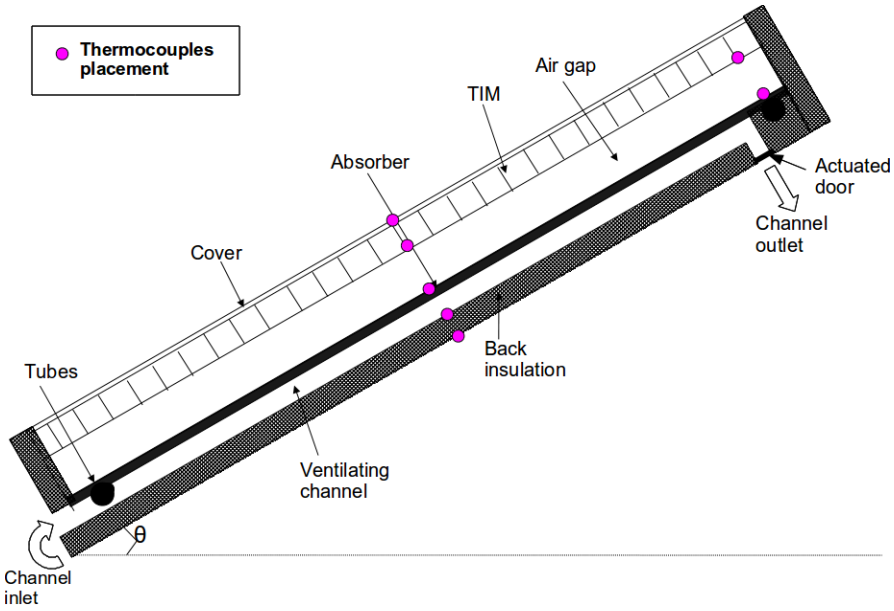

Figure. 1: Cross section of the designed FPSC with ventilating channel and honeycomb cover

2.2. Design of the overheating protection system

In order to achieve the goal of stagnation resistance, several possible solutions were studied and compared. The overheating protection system to choose, should not present any technical risk, should be cheap and has to work safely throughout the lifetime of the collector (i.e. 20 years).

Different alternatives for overheating protection systems have been considered:

- Use of glass capillaries TIM instead of plastic TIM: the price of this material is up to now still too high for a practical application.
- Heat exchanger fluid/air for the extraction of excess heat: this solution has been excluded for its high cost and for security reasons. In fact, the protection system has to be located inside the collector itself.
- Use of Phase Change Material PCM filled in a tank located inside the collector: this solution has been excluded because the PCM has a delay which can leads to the melting of the TIM. Moreover, by introducing a PCM module, the total weight of the collector increases considerably which is not favorable for commercial purposes.
- Use of mechanical shading devices (roller blind, venetian blinds): this solution has been excluded due to the high cost of these components.

As a solution to this problem, a ventilation channel located between the absorber and the back insulation of the solar collector is proposed. This channel has the function to protect the collector in stagnation conditions by introducing ambient air in the zone under the absorber allowing the natural convection cooling of the absorber plate.

The ventilation channel is designed to be located under the absorber and not upon it in order to avoid the entrance of dust and moisture to the collector. Otherwise, impurity can accumulate on the TIM and the glazing which can considerably reduce the transmittance of the transparent cover and thus decreasing the global efficiency of the collector.

This channel has an inlet and an outlet located at its opposite ends. The inlet of the channel is located at the bottom of the collector and is always opened. The outlet is located at the rear top of the collector and should be controlled by a door that opens before reaching the maximum resistance temperature of the TIM and closes at some specified temperature under this value.

When the door opens, it allows the ambient air to circulate along the channel entering from the bottom and exiting from the top. However, natural convection occurs by contact of the ambient air with the absorber back surface which is driven passively to the outside by a temperature induced density gradient. Once the collector is cooled and its operation temperature decreases under prescribed temperature, the outlet door should close for restricting the circulation of air through the channel.

For the proposed design, a shutting device should be located at the outlet that actuates at high temperatures to open the outlet door. This way, the ventilation channel will introduce additional thermal losses permitting to avoid reaching very high temperatures while these thermal losses remain negligible during normal operations (since the outlet door will be closed and no air circulation occurs).

Concerning the shutting device, different types of actuators have been considered:

- **Wax actuator:** When the collector is cold, the door is closed and prevents the flow of air into the channel. The rise of the collector temperature by solar radiation will heat the air in the channel; the wax actuator expands opening the door and allowing the air flowing inside the collector. This will provide evacuation of excess calories.
- **Shape memory alloy actuator**: It allows more or less, or completely prohibits the passage of air into the channel as a function of temperature. As long as the temperature inside the collector is low, the actuator is retracted and the door is kept closed. There is no air circulation in the channel. When the collector reaches a certain temperature, the actuator expands and will open the door allowing the air to flow through the channel. Example: start opening at 90°C and late opening at 100°C.
- **PV actuator**: It is possible to use a small photovoltaic cell with battery that powers an electric motor for operating the channel door.

The three possibilities have been analyzed with respect to their feasibility. For reasons of assembly simplicity, economic price and availability in the European market, we have chosen the second option. A Shape Memory Alloy (SMA) actuator is a material that when deformed, within limits, will regain its original shape when heated (or cooled). SMA undergoes a solid-to-solid phase transformation and exhibit very different properties above and below their transition temperature. This solid-to-solid phase transformation from the martensite to austenite phases gives a SMA spring with two very different spring constants. SMA spring is one form of thermo-variable rate spring.

A NiTi (Nickel Titanium) SMA spring was used as actuator. Its actuation starts at 90-100°C and be completed at 120°C. The SMA spring is placed in the back of the absorber plate and directed toward the outlet of the channel. When the temperature inside the air channel rises up to 90°C; the SMA spring begins to open to activate the door. When the door opens, the air flows through the channel to cool the collector. When the internal temperature decreases below <90°C, the SMA spring begins to compress drawing the door to its initial closed state.

3. The numerical model

3.1. General model:

A general numerical model is designed for the prediction of the thermal performance of the described solar collector. The proposed mathematical model is based on the resolution of the steady state energy balance equations of the different collector components. The integration of the different phenomenologies taking place in each element is carried out by means of a multi-layer approach. Each zone of the collector (Cover, TIM, Absorber, Air gap, Air channel,..) is coupled with its neighbor zones through a global algorithm. Each

zone can be simulated by means of a global model (for fast calculation) or a high level model (for full resolution of the governing equations). Depending on the desired level of modeling, the algorithm is able to choose among the different levels for each zone.

3.2. TIM model

The TIM is the most complicated part to be modeled in the collector. In a first step, it was modeled by means of a simplified analytical model using the decoupled mode analysis described by Platzer 1992-b. This model assumes an effective conductance of the TIM and then calculates the radiative heat transfer through the TIM.

In a second step, a high level model was developed. This high level model solves numerically the energy equation coupled with the radiative heat transfer equation to obtain the coupled heat transfer through the TIM.

The heat transfer in TIM is usually dominated by the radiative heat transfer because of the semi transparency of its materials to radiation. The second mechanism of heat transfer is the convection which is usually suppressed by TIM since the cells are designed such that its characteristic dimension is smaller than a critical length determined by the dimensionless Rayleigh number, plate distance and temperatures. The third mechanism of heat transfer is conduction through the walls and through the gas filling. This type of heat transfer depends on the type of the TIM materials.

Radiation, conduction and convection (if present) are coupled heat transport modes in transparent honeycomb insulation materials. However, Platzer 1992b showed that when the honeycomb cell aspect ratio is large enough and if at least one of the ends of the honeycomb cells is closed to prevent inter-cell convection rolls, the convection can be suppressed for typical collector conditions.

Only few studies have examined the coupled radiative and conductive numerical problem across honeycomb materials. The most important study is that of Hollands et al 1984 who studied experimentally and numerically the total heat transfer across the honeycomb panel. They used the Net Radiation Method (NRM) for the calculation of the radiation transport (with diffuse or specular boundaries) and solved the coupled problem by a finite difference algorithm. Their one dimensional model based on gray surfaces and specular side walls yielded results within 6% of measurements.

Arulanantham and Kaushika, 1996, also studied the coupled radiative and conductive heat transfer across the TIM with similitude with the coupled heat transfer through a plane layer of absorbing emitting gas. The governing equations for one dimensional heat transfer were formulated using exponential kernel approximation.

Schweiger, 1997, used the Monte Carlo Method to calculate the heat transfer coefficient of a hexagonal honeycomb by approximating it as a two dimensional slat structure.

Mathematical and numerical analysis

The TIM structure consists of a cellular array of repetitive nature. This specific structure allows some simplifications (Hollands et al 1984). In fact, any incident ray, if not being parallel to one of the cell walls, will hit the walls of the honeycomb that can absorb, emit, transmit or reflect the incident radiation.

If we analyze every cell separately, identical conditions are encountered. In fact, for every outgoing ray transmitted by a cell wall, there is another incoming ray which penetrates from the adjacent cell traveling along the direction into which a perfect mirror would have reflected the original leaving ray (see figure 2).

Taking this into account, we can consider a single isolated cell with opaque and adiabatic walls having a fictitious reflectivity equal to the sum of the reflectance and transmittance of the wall itself.

Depending on the cell walls, the reflectivity should be treated as diffuse or specular. If the wall surface is rough, scattering will be

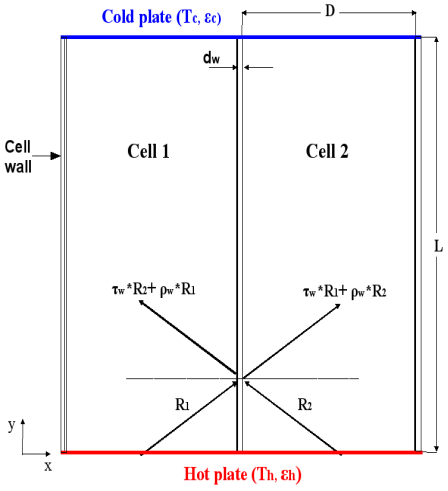

Figure. 2: geometry of honeycomb structure

strong and the diffuse model can be used. On the other hand, if the wall surface is smooth, it will be better to use the specular model.

The three dimensional combined radiation and conduction heat transfer across one isolated cell of the honeycomb is fully described by the energy equation:

$$-\lambda\nabla^2 T + \nabla q_R = 0 \quad \text{(eq. 1)}$$

Where the divergence of the radiative heat flux is expressed by equation 2 and it relates the energy equation with the radiative transfer equation.

$$\nabla q_R = \kappa(4\pi I_b - G) \quad \text{(eq. 2)} \quad \text{Where } G = \int_{4\pi} I(r,\vec{s})d\Omega \text{ is the incident radiation, } \kappa \text{ is the absorption}$$

coefficient of the medium, and I_b is the black body intensity.

The Radiative Transfer Equation:

The governing equation for radiative transfer of absorbing, emitting and scattering medium is an integro-differential equation for the radiative intensity. It is written as:

$$\frac{dI(r,\vec{s})}{ds} = \kappa I_b(r,\vec{s}) - \beta I(r,\vec{s}) + \frac{\sigma_s}{4\pi}\int_{4\pi} I(r,\vec{s}')\Phi(\vec{s}',\vec{s})d\Omega \quad \text{(eq. 3)}$$

where β is the extinction coefficient, σs is the scattering coefficient, Φ is the scattering phase function, and Ω is the solid angle.

The boundary conditions for the intensity in case of a diffusely emitting, specularly reflecting opaque surfaces are described by equation :

$$I(r_w,\vec{s}) = \varepsilon(r_w)I_b(r_w) + \frac{\rho_d(r_w)}{\pi}\int_{n.\vec{s}_i<0} I(r_w,\vec{s}')|\vec{n}.\vec{s}'|d\Omega + \rho_s(r_w)I(r_w,\vec{s}_s) \quad \text{(eq. 4)}$$

where $\vec{s}_s$ is the specular direction defined as the direction from which a light beam must hits the surface in order to travel into the direction of $\vec{s}$ after a specular reflection.

The Finite Volume Method

The majority of radiative heat transfer analyses use different solution methods for solving the equation of transfer, among them: the Spherical Harmonics Method, the Discrete Ordinates Method, the Zonal Method, the Monte Carlo Method, the Finite Volume Method, etc. Among these methods, the FVM have focused attention due to its capability to solve the radiative transfer equation (RTE) in multidimensional emitting, absorbing and scattering media (for details of this method see Chai et al, 1994 and Raithby and Chui, 1990).

The FVM is able to ensure radiative energy conservation and uses moderate computational resources. Besides, it permits to capture the collimated directions without any constraint and allows to model specular reflection boundaries due to its symmetric angular discretization.

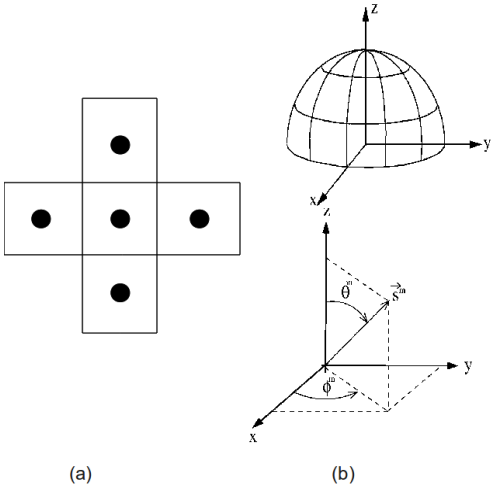

Figure. 3: Shematics of a control volume (a) control angle (b)

It can be applied with the same computational grids as those used to compute fluid flow and convective heat transfer.

In the FVM, space within the interior of the domain of interest is subdivided into discrete nonoverlapping volumes (see Figure 3-b), and a single node is located centrally within each volume. Since direction is also an independent variable, it is subdivided into N^l discrete solid angles of size Ω^l, l=1,2,3,..., which sum to 4π. The objective of the FVM is to find I^l_p, the intensity at each node P associated with each discrete bundle Ω^l.

General algorithm

The energy equation is discretized using the finite volume technique; the spatial discretization is carried out using uniform grids. The solutions of the RTE are obtained using the FVM. The coupled conduction and radiation problem is solved through the following algorithm: first initial value for the radiative heat flux is

assumed. Second, the energy equation (equation 1) is solved to obtain the temperature map. Then, we solve the RTE (equation 3) to obtain the intensity map. We calculate the divergence of the radiative heat flux (equation 2) and set the new boundary conditions (equation 4). The process is repeated until convergence on temperatures and radiative heat fluxes.
Once we get the numerical solution on the TIM, the conductive and radiative heat fluxes are post process computed and then used by the balances equations in the global model of the collector.

3.3. Air Gap model

The heat transfer between two parallel plates inclined at some angle to the horizon is investigated by various authors and it is well explained by Duffie and Beckman 1980.
One of the most reliable correlations for closed rectangular cavities with high aspect ratio is that given by Hollands et al 1976 which relates Nusselt number and Rayleigh number for tilt angles from 0 to 75° as:

$$Nu = 1 + 0.44\left(1 - \frac{1708(\sin(1.8\theta)^{1.6}}{Ra.\cos(\theta)}\right)\left(1 - \frac{1708}{Ra.\cos(\theta)}\right)^{+}\left(\left(\frac{Ra.\cos(\theta)}{5830}\right)^{1/3} - 1\right)^{+} \quad \text{(eq. 5)}$$

This correlation has been used for the calculation of the heat transfer coefficient in the air gap of the collector.

3.4. Air channel model

A great variety of theoretical and experimental works has been done to study ventilation by natural convection in rectangular cavities with high aspect ratio. Bar-Cohen and Rohsenow, 1984, developed correlations for fully developed flows in a symmetric isothermal and isoflux channel as well as in a channel with an insulated wall. Fedorov and Viskanta, 1997, studied turbulent natural convection heat transfer in an asymmetrically heated, vertical parallel-plate channel. In their work the low Reynolds number k-ε turbulence model is used to simulate the turbulent flow and then to establish their correlation. Sakonidou et al, 2008, developed a model that estimates the tilt of a solar chimney that yields the largest natural air flow. For calculating the convective heat transfer, they used the correlation given by VDI-Warmeatlas 1991 valid for inclination below 75°. Chami and Zoughaib, 2010, modeled natural convection in a pitched thermosyphon system in building roofs with experimental validation using particle image velocimetry. They established a correlation for the inter-plate spacing range between 0.01 and 0.03 m and the inclination range from 30° to 45°.
The different correlations were tested; the correlation adopted by Sakonidou et al, 2008 was found to correlate well for our case and is thus used in the simulation of the channel as a low level model.

$$Nu = 0.56(Ra.\sin(\theta))^{1/4} \quad \text{(eq. 6)}$$

$$Nu = 0.56(Ra.\sin(\theta))^{1/4} + 0.13(\mathrm{Ra}^{1/3} - \mathrm{Ra}_c^{1/3})$$

Where Ra_c is a critical Rayleigh number defined as: $\log(Ra_c) = 8.9 - 0.00178(90 - \theta)^{1/4}$

It has to be noticed that the turbulent air flow in the ventilation channel is under simulation by means of a high order level. This high order model uses a LES simulation of the turbulent flow in three dimensional coordinates. This model will allow us in the near future to establish our own correlations for the ventilation channel.

3.5. Absorber model

A one dimensional step by step model was developed for the simulation of the absorber. Nevertheless, this high level model is not yet integrated to the global model of the collector. In this work, for the simulation of the absorber we established its energy balance equation assuming a uniform temperature and a prescribed heat transfer coefficient with the circulating fluid.

4. Experimental tests

The experimental tests were conducted in order to verify the performance of the designed overheating protection system, calculate the solar collector efficiency as well as to validate the developed numerical model. The validation consists of comparing the experimental versus the numerical results.

4.1. Experimental test facilities

For the measurement of the fluid temperature at the inlet and outlet of the collector and inside the collector,

PT100 platinum thermoresistances and type K (Chromel/Alumel) thermocouple probes were used, respectively. The placements of the thermocouples within the solar collector are shown in figure 1. All the PT100 and the thermocouples were calibrated using a reference probe. The measurement error is estimated to be ± 0.06 and ±0.3 for the PT100 and the thermocouples respectively. The meteorological conditions (total and diffuse solar radiation and wind velocity) were continuously measured during all the tests. The used Kipp & Zonen pyranometer has an error of ± 0.5%.

For testing the solar collector, the test bank of the CTTC was used. The test bank uses pressurized water as working fluid, being able to perform tests for up to 150°C and 8 bars, as the limiting conditions. This test bank allows a controlled (programmable) mass flow rate and a controlled collector inlet temperature. The used flow meter has an estimated error of 0.05%. All measurements were automatically recorded using an Agilent 34970A data logger.

The errors on the determination of the heat losses and the efficiency, resulting from uncertainties in the measurements of temperatures, solar radiation and mass flow rate were calculated using the logarithmic differential.
The conducted experimental tests are the efficiency test, the stagnation conditions test and the thermal heat loss test.

4.2. Indoor measurements

The thermal heat loss test is not part of the ISO standards; however it is useful to define steady heat loss as a function of operating temperature. Heat loss measurements were carried out indoors with zero incident radiation in order to determine the collector heat losses. All measurements were carried out at constant inlet temperature and with a constant mass flow rate close to the optimum value of Re=2300 (0.042 Kg/s). The data were taken after the system reached a steady state in intervals of 10 seconds during 30 minutes.

In order to check up on the efficiency of the overheating protection system, the prototype has been tested in different operation modes (See figure 4):

Open channel: the ventilation channel is totally opened.
Active actuating door: the ventilation channel door is activated.
Inactive actuating door: the overheating protection system is deactivated.

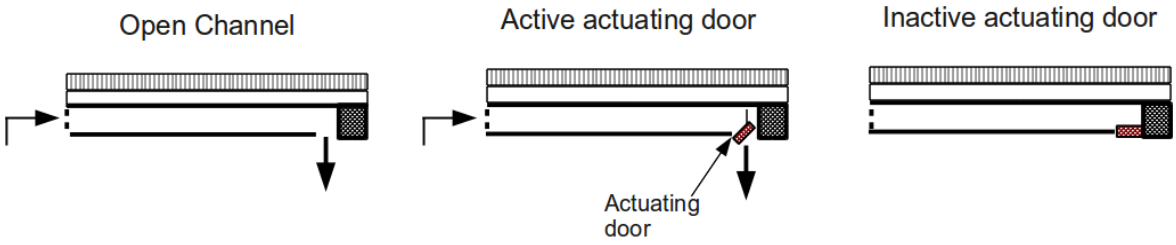

Figure. 4: Operation modes of the ventilation channel

Figure 5 shows the heat losses in terms of the temperature difference between the thermal fluid and the ambient (T_{av}-T_{amb}). It can be observed that when the channel is closed the collector heat loss curve is minimum. In this case, the heat losses from the channel are negligible. When the channel is opened, the heat losses from the air channel become very important and represent approximately 40% of the total losses of the collector.

When the channel door is active, the heat losses, at low operation temperatures, are similar to those obtained with closed channel. However, when the temperatures inside the collector increase and the shape memory allow spring reaches 90°C, the channel door start to open to let heat evacuating from the back of the collector. When the SMA spring is completely opened, we see that the heat loss curve come closer to the opened channel curve.

These results show that the designed overheating protection system gives the desired effect that is to increase the collector heat losses only for high operating temperatures. This increase in the heat losses allows refreshing the collector to protect the TIM from achieving high temperatures.

4.2. Outdoor measurements

Outdoor measurements were done in Terrassa, Barcelona, Spain. The collector was exposed, facing the south with an inclination of 41° (latitude of Barcelona), to solar radiation in the midday hours when the beam radiation is high and nearly normal to the collector plane.

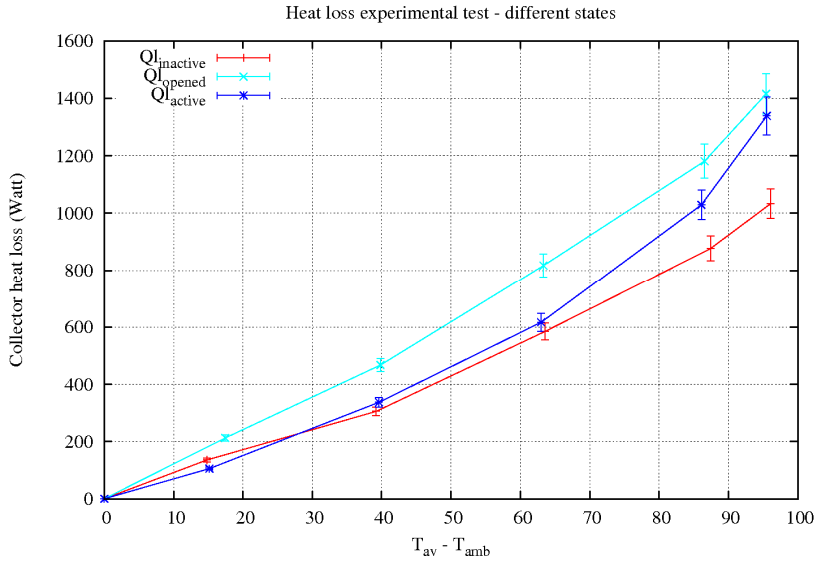

Figure. 5: Heat loss curve of the collector for different operation modes

Steady state efficiency test

The basic method of determining collector performance is to make the outdoor steady-state efficiency test. During this test, the international standard procedure ISO 9806-1 was followed. The Experimental efficiency curve is presented in figure 6. Sixteen points are shown, four for each temperature range.

The scatter in the results was expected due to the temperature dependence, wind effects, and angle of incidence variation during the test. The efficiency is expressed by the following equation obtained using the least square method:

$$\eta = 0.732\text{-}7.19\ (T_{av}\text{-}T_{amb})/G \qquad \text{(eq. 7)}$$

where G is the total solar radiation in the collector aperture. The coefficient of determination R^2 is of 0.98 indicating a good fit with the data. It has to be noted that the tested collector has not a very good selective coating of the absorber which explains the relatively low efficiency.

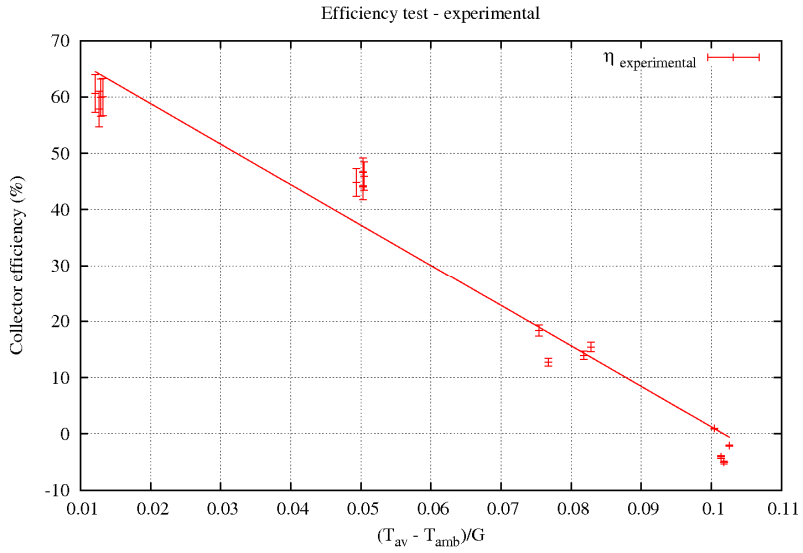

Figure. 6: Experimental efficiency curve of the collector

Stagnation conditions test

The collector prototype has been exposed to the solar radiation without circulation of water through the absorber during June 2011. The solar radiation and the temperatures inside the collector have been continuously measured. The tests have been performed in a clear sky day from 10 a.m to 5 p.m. During the tests, the temperatures in different locations of the collector as well as the solar radiation were measured continuously every 30 seconds.

Results for two testing days (22 and 28 June 2011) are shown in figure 7. The solar radiation during the tests period is also presented in figure 7. These days were chosen among the hottest days in the year in order to check up on the efficacy of the designed overheating protection system. The solar radiation and the ambient temperature in both test days were very similar.

The first test was done keeping the channel door closed during the entire test. In the second test, the designed thermally activated door was activated.

During the first test, when the channel was kept permanently closed, the temperature of the different components of the solar collector was seen to increase continuously until reaching temperatures of the TIM more than 140°C which is the maximum temperature that can support the TIM before starting to melt (this information was given by the TIM constructor). The stagnation test was thus interrupted.

This first test has shown very clearly that a FPSC with TIM and without overheating protection system cannot withstand the stagnation conditions and the TIM would melt. Consequently, the designed overheating protection system is very important to protect this type of solar collectors.

During the second test, the designed thermally activated door was operational. As the solar radiation increased, the temperatures of the different components of the collector were observed to increase. The TIM temperature was the hottest point in the collector during the entire test. It was seen to reach a maximum temperature of 137°C in the midday.

The operation of the overheating protection system was verified by visual inspection: when the air channel temperature reached about 90°C, the SMA spring was seen to extend opening the channel door and letting the air circulating inside the collector. Later in the day, as the solar radiation decreased and the temperature in the channel dropped, the SMA spring was seen to decompress driving the channel door to its initial closed state.

This second test showed the effectiveness of the overheating protection system and demonstrated that high temperatures in the TIM can be limited and thus protect the collector in stagnation conditions.

5. Simulation results

The balance equations of the solar collector were established. An iterative method for solving the system of equations was used. The heat transfer coefficients were first calculated using initial guess values of temperatures. Next, the balance equations were solved to obtain the new temperatures. This completed one iteration cycle, cycles being repeated until convergence. All the presented simulations were obtained using low level models for the different components (TIM, air channel and absorber).

5.1. Heat loss comparison

The heat loss curve for zero incident radiation in terms of (T_{av} -T_{amb}) has been calculated using the numerical model described above. The values obtained with the model are compared with the experimental ones and are depicted in figure 8.

Most outstanding conclusions arisen from the discussion of these results are:

- Good agreement between numerical and experimental data is observed in the heat loss, where the highest differences are below 5% for the case of closed channel and below 8% for the case of an opened channel.
- General tendencies of the numerical and experimental data are similar and no relevant effects are observed for low or high levels of temperatures.
- The error found between experimental and numerical results can be explained by the correlations

used in the model.

- The experimental as well as the numerical results confirm that the prototype in stagnation conditions and with the ventilation channel opened is able to lose (evacuate) the heat necessary to prevent the collector from overheating.

5.2. Efficiency comparison

Experimental efficiency curve compared with numerical curve obtained with the developed simulation program are given in figure 9. The meteorological data measured during the test were used as inputs in the numerical simulation of the collector (Solar radiation, wind, ambient). Similar tendencies are observed with the numerical and experimental results. The model overpredicts the measured efficiency by no more than 3%.

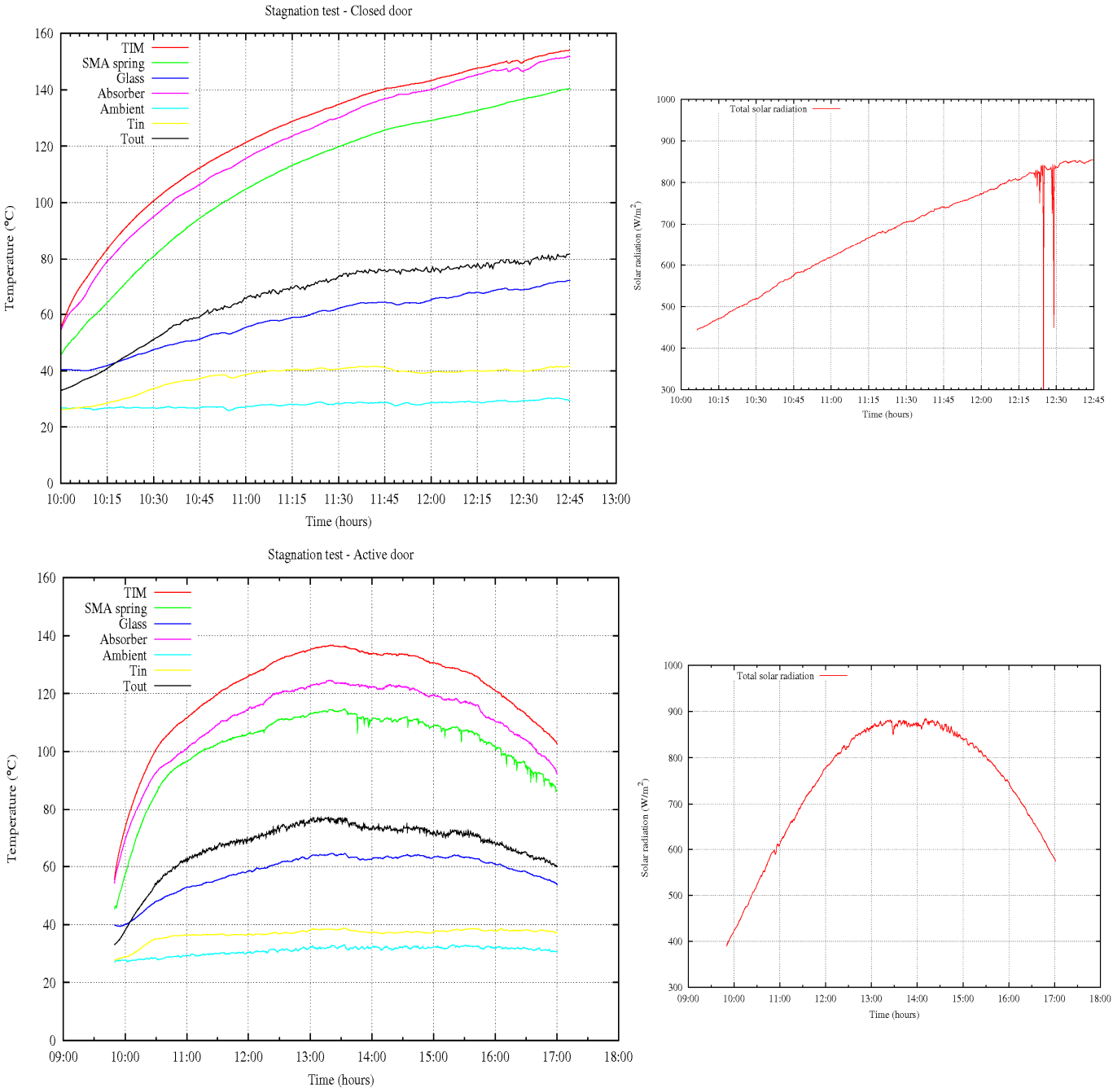

Figure. 7: Results for the stagnation conditions test. Top: closed channel, Bottom: Active channel door, Left: Temperatures of the different components of the collector, Right: Solar radiation recorded during the tests

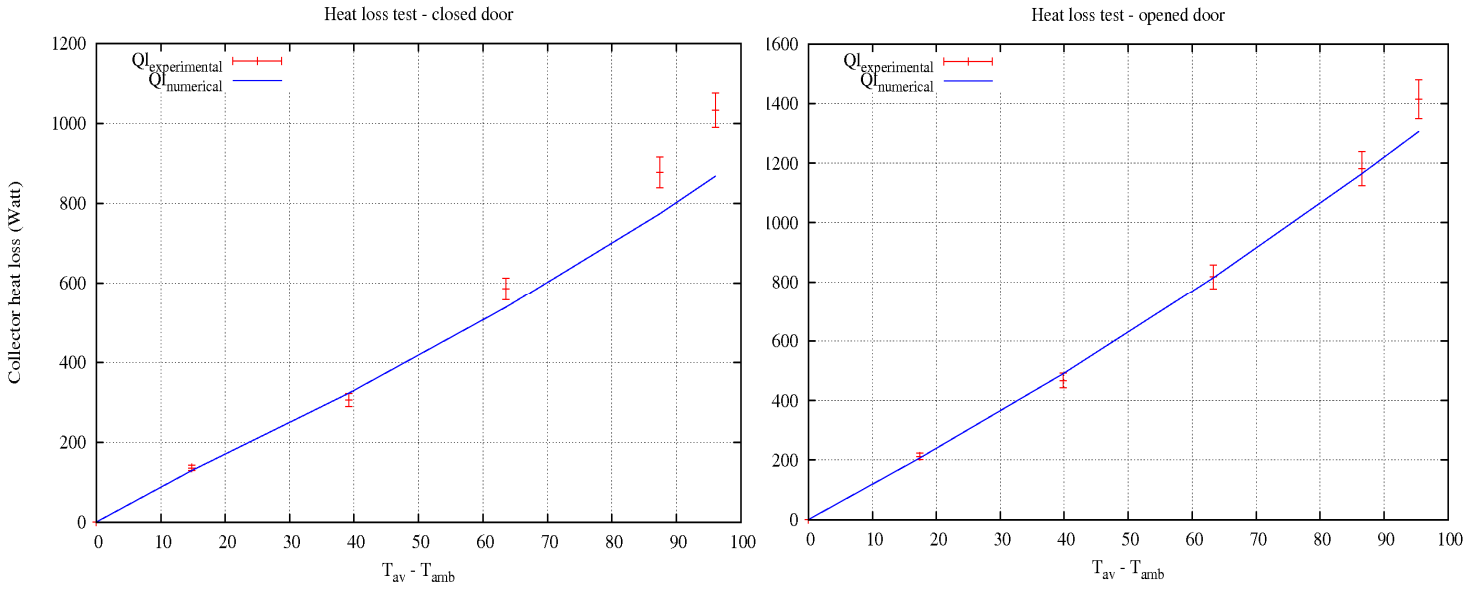

Figure. 8: Numerical vs experimental comparison of the heat loss curves. Left: closed channel, Right: Opened channel

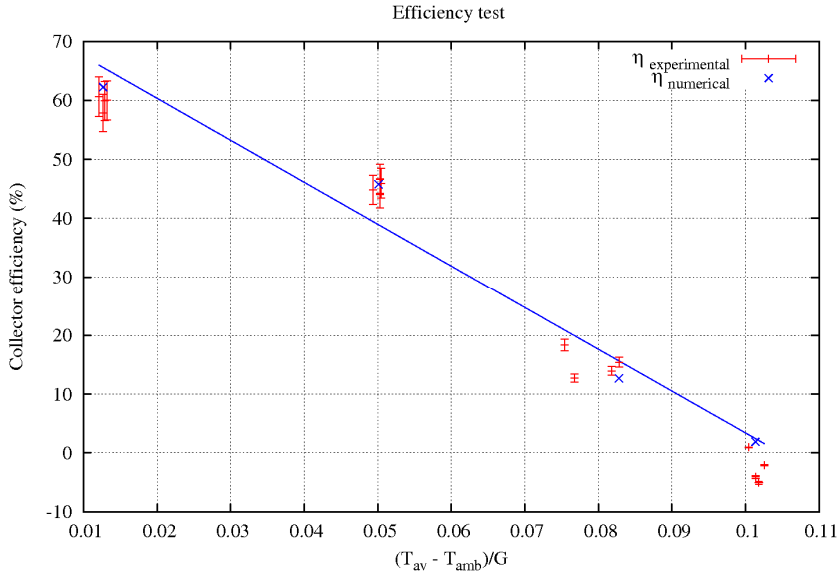

Figure. 9: Numerical vs experimental comparison of the collector efficiency curves

5. Conclusions

This work has addressed the development of a flat plate solar collector with transparent insulation material and overheating protection system. A prototype has been constructed and tested according to ISO procedures including steady state efficiency and heat loss test. A numerical simulation program has also been developed able to predict the efficiency and heat losses of the collector by a discrepancy that does not exceed 3% and 8% respectively.

The designed ventilation channel with thermally actuated door has shown its ability to maintain low enough temperatures in the collector preventing the collector from stagnation conditions.

This work has been a step forward to make the flat plate solar collectors with TIM a commercial product competing to other products already available in the market such as evacuated tube collectors with expected lower costs.

Acknowledgements

This work is financially supported by the Spanish Agency of International Relations (AECI) and by the Generalitat de Catalunya, CIDEM (ref. VALTEC08-1-0018).

6. References

Platzer, W.J. Calculation procedure for collectors with a honeycomb cover of rectangular cross section., 1992a. Solar Energy. 48-6, 381-393

Platzer, W.J. Total heat transport data for plastic honeycomb-type structures., 1992b. Solar Energy. 49-5, 351-358.

Rommel, M. and Wagner, A. Application of transparent insulation materials in improved flat-plate collectors and integrated collectors storages., 1992. Solar Energy. 49(5), 371-380.

Schweiger, H. Optimization of solar thermal absorber elements with transparent insulation., 1997. PhD Thesis, Universitat Politècnica de Catalunya.

Kaushika, N. D. and Sumathy. K. Solar transparent insulation materials: a review., 2003. Renewable and Sustainable Energy Reviews. 7, 317-351.

Arulanantham, M. and Kaushika, N. D. Coupled radiative and conductive thermal transfers across transparent honeycomb insulation materials., 1996. App. Thermal Eng. 16(3), 209-217.

Hollands, K.G.T. and Raithby, G. D. and Russel, F.B. and Wilkinson, R.G. Coupled radiative and conductive heat transfer across honeycomb panels and through single cells., 1984. 27-11, 2119-2131.

Chai, J.C. and Lee, H.S. and S.V. Patankar. Finite Volume Method for Radiation Transfer., 1994. Journal of Thermophysics and Heat Transfer., 8, 419-425.

Raithby, G.D. and Chui, E.H. A Finite-Volume Method for Predicting a Radiant Heat Transfer in Enclosures With Participating Media., 1990. Journal of Heat Transfer. 112, 415-423.

Bar-Cohen, A. and Rohsenow, W. M. Thermally optimum spacing of vertical, natural convection cooled, parallel plates., 1984. Journal of heat transfer. 106, 116-123.

Fedorov, A. G. and Viskanta, R. Turbulent natural convection heat transfer in an asymmetrically heated, vertical parallel-plate channel.,1997. International Journal of Heat and Mass Transfer. 40(16), 3849-3960.

Sakonidou, E. P. and Karapantsios, T. D. and Balouktsis, A. I. and Chassapis, D. Modeling of the optimum tilt of a solar chimney for maximum air flow., 2008. Solar Energy. 82, 80-94.

Chami, N. and Zoughaib, A. Modeling natural convection in a pitched thermosyphon system in building roofs and experimental validation using particle image velocimetry.,2010. Energy and Buildings., 42, 1267-1274

ISO9806-1. Test methods for solar collectors., 1994.

Goetzberger, A. and Rommel, M. Prospects for integrated storage collector systems in central Europe., 1987. Solar Energy., 39, 211-219.

Hollands, K. G. T. and Unny, T. E. and Raithby, G. D. and Konicek, L. Free convection heat transfer across inclined air layers., 1976. J. Heat Transfer., 98, 189.

Duffie, J.A. and Beckman, W.A. Solar engineering of thermal process., 1980. John Wiley and Sons, Inc., 2nd edition